Study on Pre-Compaction of Pavement Graded Gravels via Imaging Technologies, Artificial Intelligent and Numerical Simulations

Chonghui Wang[a,d], Xiaodong Zhou[b], Pengfei Liu[a]*, Guoyang Lu[c], Hainian Wang[d], Markus Oeser[a,e]

a Institute of Highway Engineering, RWTH Aachen University, 52074, Aachen, Germany
b Dept. of Civil and Environmental Engineering, Michigan Technological University, 49931, Houghton, USA
c Dept. of Civil and Environmental Engineering, The Hong Kong Polytechnic University, Hong Kong
d School of Highway, Chang'an University, 710064, Xi'an, China
e Ferderal Highway Research Institute, 51427, Bergisch Gladbach, Germany

Abstract:

Pavement compaction cannot be neglected during the motorway manufacture stage because it can determine pavement service quality and durability. Concerning the compaction scenario, the paving compaction is responsible for offering the preliminary strength of the pavement. Ignoring paving compaction quality control can lead to over compaction. This paper introduces an integral system to study and simulate the paving compaction of asphalt motorways in Discrete Element Model two-dimensional (DEM2D). This method includes the whole procedure from aggregate image acquisition database establishment to the DEM2D simulation of paving compaction. To this end, this study fulfils the creation of the aggregate database applied in DEM via the Aggregate Image Measuring System (AIMS) method. In addition, the artificial intelligent (AI) technology called Generative Adversarial Networks (GANs) method is proposed to expand the developed DEM aggregate database. Three different approaches are applied to calibrate the accuracy of the extended database. According to the aggregate database, the pavement paving compaction with different aggregate gradations can be simulated in DEM2D.

Keywords: pavement compaction, discrete element, image technology, aggregate, artificial intelligent, deep learning, asphalt pavement

1 Introduction

Asphalt pavement compaction is one of the key steps during motorway manufacture engineering, determining the motorway's service quality and durability. The pavement compaction can be divided into two phases during the road construction process. The asphalt pavement achieves preliminary density (pre-compaction) done by the paver in the first phase, namely paving compaction. After pre-compaction, it comes to the second phase, during which the final compaction is finished via roller compactors [1]. Therefore, the pre-compaction from the paver plus the final compaction from the rollers achieves the required density of the asphalt pavement [2]. According to the requirements of construction guidelines in different regions of the world, evaluating the quality of the asphalt pavement compaction dominantly depends on its final compaction degree. Therefore, these specifications require that the compaction evaluation is always performed after the final compaction of the roller [3]. Xu et al. has been proved by research that the overall quality of road compaction can already be ensured through sufficient preliminary compaction by the paver, which has a great contribution to the final compaction (e.g., reducing the roller passes) [4]. However, if the compaction degree done by paver is higher than its expected value, the roller compaction scenarios must be altered. Otherwise, the final compaction can easily lead to over-compaction [5].

Recently, several innovative studies have been used for asphalt compaction such as intelligent compaction [6,7] and numerical simulation. The simulation methods such as finite element method (FEM) and discrete element method (DEM) have been commonly applied to simulate the macroscopic and microscopic mechanical and deformation properties of materials, including asphalt pavement materials [8–12]. In order to simulate the macroscopic dynamic response behavior of asphalt surface during rolling, the simulation method of continuum mechanics (i.e., FEM) can be used to solve the problem, such as [13]. Liu et al. analyzed and compared the mechanical and deformation properties of asphalt mixtures compacted by different methods through the FEM model [14,15]. In general, the finite element method is an efficient and practical solution for studying isotropic materials.

However, when the asphalt mixture is studied as an anisotropic or discrete material, the computational cost and efficiency of FEM will increase considerably [16].

Since the introduction of DEM by Cundall in the 1970s [17,18], this method has been very popular in the simulation study of anisotropic materials. DEM can mainly be used to simulate the dynamic properties of granular materials. This simulation method is very helpful for the intuitive understanding of the dynamic properties of building materials [19–21]. Furthermore, the importance of road aggregates to the overall performance of the mixture has been emphasized in numerical simulations [22–24] and laboratory tests [25–31]. In addition, Liu et al. have modified the method of generating aggregates. They have utilized DEM to study the sieving experiments of aggregates with real shape information [19], but generating "real aggregates" takes more computational time. For the contact model, Erik Olsson et al. have developed a DEM framework for asphalt compaction in 2019. The binder phase of asphalt is defined by adding a viscoelastic around the surface of each aggregate [32]. This surface layer has proper mechanical behaviors representative for the bitumen at different temperatures, especially at the thermal condition during the compacting process. This proposed method is quite efficient and practical since the model does not need to regard the bitumen as small particles which take up a large part of the calculation.

The morphological properties of aggregate have a dramatic influence on pavement compaction. Therefore, the image information of aggregate is supposed to be captured and put into the DEM simulation. In recent years, the acquisition and processing technology of digital pictures has been advanced and developed. And many methods have been derived to measure and study the morphological properties of aggregates. For example, X-ray CT is one of the most common methods for representing and analyzing pavement aggregates [8]. Also, some researchers tried to use laser scanning devices to measure aggregate shapes [33,34]. Liu et al. has applied the optical scanner to describe the morphological characteristics and compared this method to X-ray CT technology [35]. Some other studies took efforts to scan the aggregates using AIMS [36,37].

The mechanical properties of aggregates are affected by many factors, among which the uncertainty of particle size and morphology distribution of aggregates makes them more complicated. Therefore, the sample size of the aggregate database needs to be sufficient to ensure the random generation of aggregates. But the development of an aggregate database could be very time-consuming and energy-consuming if relying on traditional methods. In the past decades, the application of machine learning has been a concerning issue, including in the pavement field. Deng et al. have used a neural network model to identify the bridge structural damage [38]. Zhang et al. have used Generative Adversarial Networks (GANs) to learn and identify road surface cracks [39]. Inspired by this, the problem of randomly generating many digital aggregate images can be solved by machine learning methods. Furthermore, GANs, one of the machine learning methods, can enrich aggregate morphology databases and significantly reduce aggregate shape processing time [40–45].

2 Objective and methodology

Concerning the issues mentioned above, this paper introduces an integrated system developed by the author, which includes the whole procedure from aggregate image acquisition, database establishment, to the DEM2D simulation of paving compaction. To this end, this study fulfils the establishment of a digital aggregation database for DEM via the AIMS method. Furthermore, the existing aggregated database is then expanded using GAN methods. The pavement paving compaction with different gradations can be simulated in DEM2D according to the aggregate database.

The research strategy can be seen as Fig. 1. First, the DEM spherical elements are generated for simulating the aggregates in pavement compaction. The contact models in terms of linear elastic and cohesive behavior are defined, respectively, according to the laboratory tests. By using image acquisition technology, different aggregate samples are collected based on their shape information. The edge points of each aggregate are recognized, and output as edge point coordinates through a

contour recognition from the image processing method. What happens next is to generate the aggregate template in DEM2D according to the contour coordinates. With the generation of the DEM aggregate template, the DEM aggregate database is then developed on the basis of this collection. Each aggregate specimen in this database has the shape index mapping from a real aggregate. For the database, some laboratory tests are conducted, such as repose angle test, to calibrate the model parameters and, on the other hand, to compare the physical property between the bulk materials with real aggregate shape and the spherical elements. The next step is to expand the aggregate database via GANs. Finally, the DEM simulation can use the aggregate database to randomly generate aggregates for pavement compaction simulation.
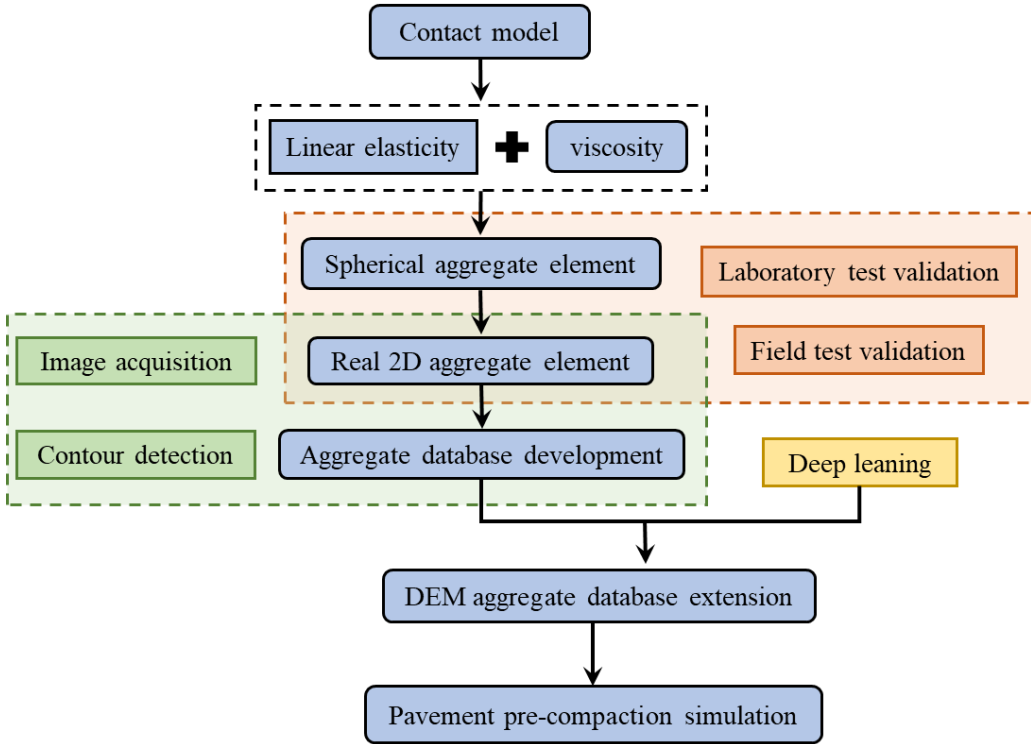

Fig. 1 Methodology

3 Development of discrete element model for pre-compaction

3.1 Contact model definition

The contact model is used to define and describe the mechanical and deformation behavior of the aggregates in contact. The contact model is defined after the model template has been generated. In

the simulation, the interaction between the aggregates at the point of contact can be simplified as a pair of elastic springs, resulting in constant normal and shear stiffness [16,17]. After defining the contact model at the local scale, elastic contact is applied to the whole model at the macro scale, and the geometry's macro deformation calculation is then performed according to the contact rules[46]. The parameters used in the contact model can be found in Table 1 [16,47–49].

However, the contact interactions mentioned here can only describe the linear elastic behavior between granular materials without the bonding effect.

Table 1 Material parameters in simulation

Density (kg/m^3)	Elastic modulus (GPa)	Stiffness ratio	Contact damp ratio	Local damping	Friction coefficient	
					Aggregate-boundary	Aggregate-aggregate
2,650	55	2.0	0.2	0	0.5	0.7

3.2 Aggregate model generation based on image acquisition technologies

The mechanical properties of bulk materials are determined by the set of local mechanical parameters and geometric characteristics of aggregates. In DEM simulations, the local mechanical parameters and geometric characteristics of aggregates determine the overall mechanical and deformation properties between aggregates. However, the DEM model generated with spherical elements cannot completely satisfy the requirement of pavement compaction simulation. This section aims to acquire the real shape of aggregate and take the shape information of aggregates as input index in the DEM numerical simulation.

Working as a digital image acquiring and processing equipment, AIMS is utilized to derive the aggregate images and to analyze their shape properties [36,50,51]. This study used AIMS to obtain angularity parameters of aggregate variation in angularity and sphericity distribution. These aggregate images are used as input for the DEM aggregate database development. The ratio of the particle dimensions, angularity are the main shape indexes of aggregate considered in the simulation. The shape of an aggregate is evaluated based on its overall outline, which can be defined and classified as flat, elongated, or flat and elongated particles.

The variation in the angle sharpness from the aggregate boundary can be quantitatively described by the gradient angle (GA) of the particles [52]. The GA index of an aggregate can be calculated through Equation 1 [51]. A higher value in GA denotes a particle with better angularity.

$$GA = \frac{1}{\frac{n}{3}-1}\sum_{i=1}^{n-3}|\theta_i - \theta_{i+3}| \tag{1}$$

where, θ indicates the angle of orientation of the edges, n indicates the total number of points and subscript i is the i_{th} gradient vector on particle boundary points.

The digital images of the aggregates are obtained and converted by image processing technology to get binary images of particles. During the digital image acquisition, image enhancement, calibration, and binarization are achieved by verifying the phase threshold, while the edge detection and measurement are finished in MATLAB.

Boundary detection is a digital image processing technology used to discriminate and obtain the outline of objectives. The boundary detection function works in MATLAB by detecting discontinuities in brightness. This function looks for places in the image where the intensity changes rapidly. In general, the edge detection algorithms include Sobel, Canny, Prewitt, Roberts, and fuzzy logic approaches [53]. The Canny algorithm is adopted utilizing MATLAB for aggregate image traction in this research. It can identify shadow areas of aggregates in binary images and detect some morphological indicators about this shadow area.

There are several steps for the procedure to obtain the identification index of aggregates and input them into DEM simulation: (1) Image acquisition: the digital information of the aggregates are captured using AIMS; (2) Edge point identification and export: the contour recognition of particles is finished in MATLAB, the export datum of particles including edge point coordinate, angularity and sphericity are then imported into the DEM2D; (3) Modular calibration: the templates of aggregate variation in morphological properties are generated in DEM2D according to the imported data; (4) The mineral type and morphological information of each particle is recorded as its identification index,

and a gene database of aggregates is developed based on this collection. Fig. 2 shows the procedure to capture information of a single particle and then import it into DEM2D.
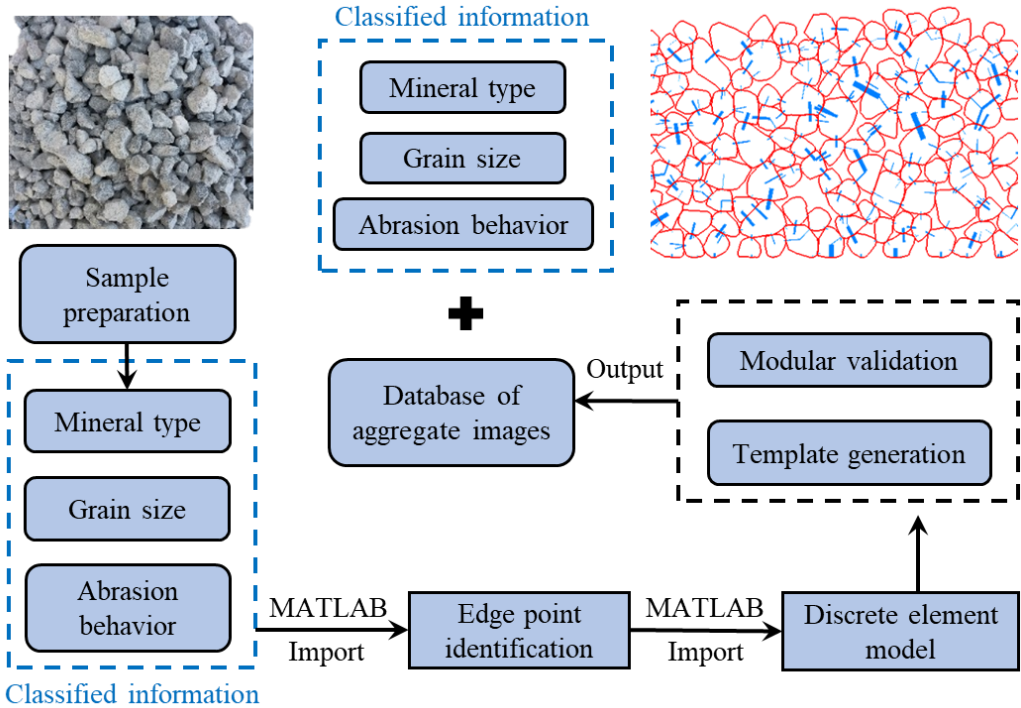

Fig. 2 Aggregate image collection and database development

After reconstructing the template of the aggregates in DEM, it can be used to generate a certain amount of aggregates with the desired gradation. The next stage is to use DEM aggregates with real shape information to simulate the mechano-deformation behavior of granular materials. A laboratory repose angle test is conducted to calibrate the model parameters, and finally, the DEM2D paving model can be developed to simulate the paving compaction.

3.3 Comparison analysis and model verification

The stiffness, density, and polishing resistance of aggregates are tested in the laboratory. And the frictional behavior of aggregates is measured and validated by the repose angle test.

The angle of repose is one sort of index to describe the surface frictional behavior of aggregates. The repose angle of aggregates is the maximum value they can naturally sustain relative angle with the horizontal direction. There are several ways available to measure the angle of repose. The one chosen in this section is the hollow cylinder method, scooping the particles into a 14-cm diameter

transparent hollow cylinder erected vertically on a horizontal platform with known roughness properties. The cylinder is then slowly raised to allow the particles to fall into a conical pile naturally. The repose angle is measured until the particles move at an equilibrium state. Then, the pile's slope is measured with a tilted protractor device in five locations. Fig. 3 shows this test in the laboratory with different grain sizes of aggregates.
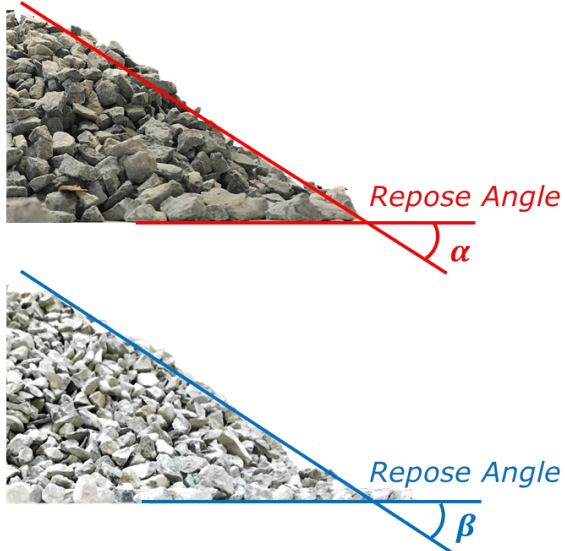

Fig. 3 Repose angle test in the laboratory for aggregates with different grain sizes. top: basalt; bottom: greywacke

Measuring the repose angle of aggregates in the simulation is also conducted to compare and validate the model. The spherical elements with rolling resistance are first generated in the DEM simulation. According to the designed gradation, the particles are developed and fall into the hollow cylinder with gravity until full. The cylinder is slowly raised vertically to allow the particles to fall into a conical pile naturally. Based on the spherical aggregate model, the DEM aggregate elements have been developed with their real image information. The repose angle is then measured until the particles move at an equilibrium state.

The whole procedure to simulate the repose angle measurement with actual particle shape can be illustrated into several steps as follows: 1) Morphology import: the templates of aggregate are generated by being called from particles database, the shape of a template is chosen each time randomly from the database with 660 types of different shapes; 2) Gradation control: the particle

templates called from the database will be multiplied by the particle size sieving coefficient so that the particle size of the template (the diameter of the external sphere) can meet the requirements of sieving size due to the certainly designed gradation [19]; 3) Generate domain setting and particle generation: the calculation domain where for generating particles is defined according to the size of the testing area, then aggregates are randomly generated in the domain through call back of particle database. The physical properties of aggregate are calculated by bubble pack algorithm, and the distribution of particle size is set based on the defined gradation; 4) Equilibrium solving of physical state: the gravity is imposed to particles after generation so that the aggregates can naturally fall into the hollow cylinder until the cylinder is full; 5) Formation of repose angle: The cylinder is slowly raised vertically to allow the particles to fall into a conical pile naturally. The repose angle is then measured until the particles move to an equilibrium state. Besides, it is worth mentioning that the simulation's friction coefficient is selected according to the repose angle test in the laboratory. The basic parameters of the cylinder and particles are provided in Table *1*.

Fig. 4 illustrates the simulation results of the aggregate repose angle test. In the DEM simulation, the particles with real shape and spherical elements with rolling resistance are simulated separately. Two different particle grain sizes (5-8 mm and 8-11 mm) are adopted in the research to study particle size's influence on the repose angle. The repose angle test of aggregates in terms of these two particle sizes is also conducted for comparison research in the laboratory. The frictional contact parameters between aggregates, cylinder surface, and bottom surface in the simulation are measured separately and validated in the laboratory. As for the particles with rolling resistance, the rolling resistance friction is set as several values for comparison, including 0.25, 0.5, 0.75, and 1.0.
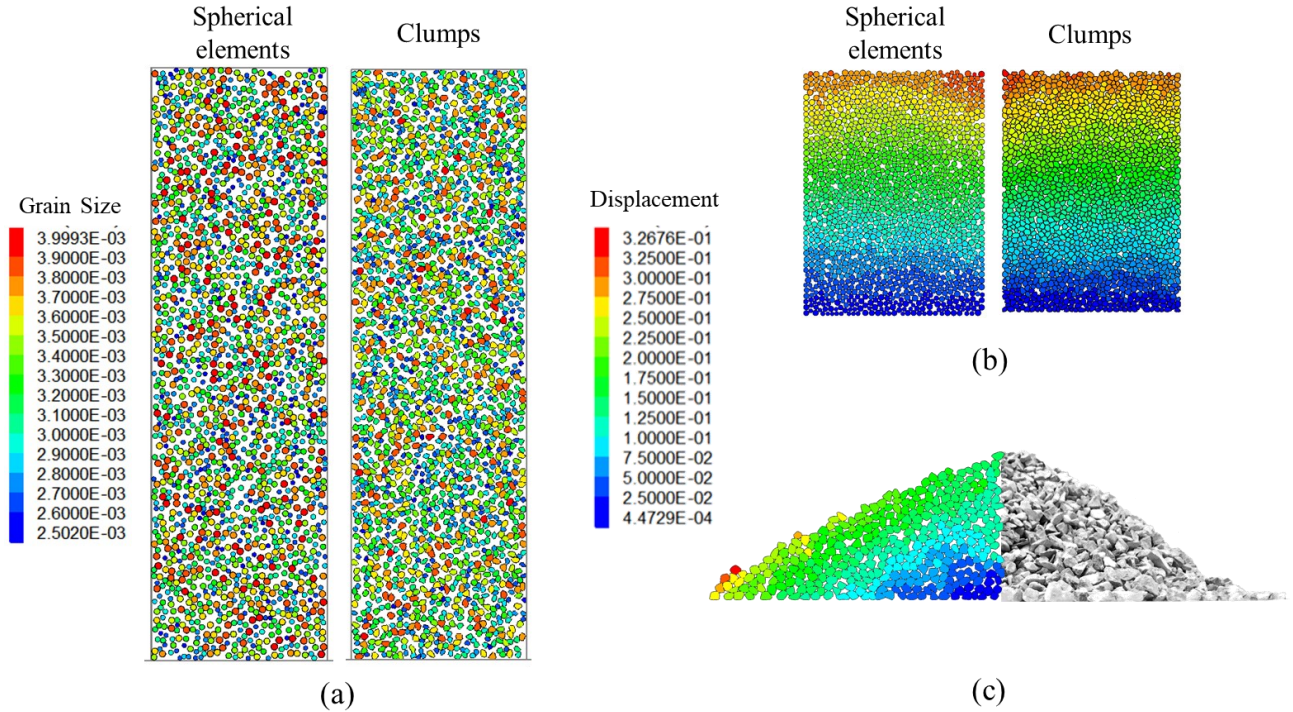
Fig. 4 The DEM simulation of response angle with the ball-based model and the clump-based model: (a) generation of model boundary and aggregates; (b) the stacking statuses of aggregates after gravity fall; (c) the response angles of the DEM models compared to laboratory test

Fig. 5 illustrates the Comparison analysis of the repose angle from laboratory test and simulation. The single-sized (5-8 mm, and 8-11 mm) granule packing simulation results are carried out using different rolling resistance friction. The spherical elements are generated with rolling resistance from $\mu_r = 0.25$ to $\mu_r = 1.0$, which can be used for comparative analyses with the results from real shape elements. Because the clumps have angularity, they are generated with no rolling resistance in the simulation.
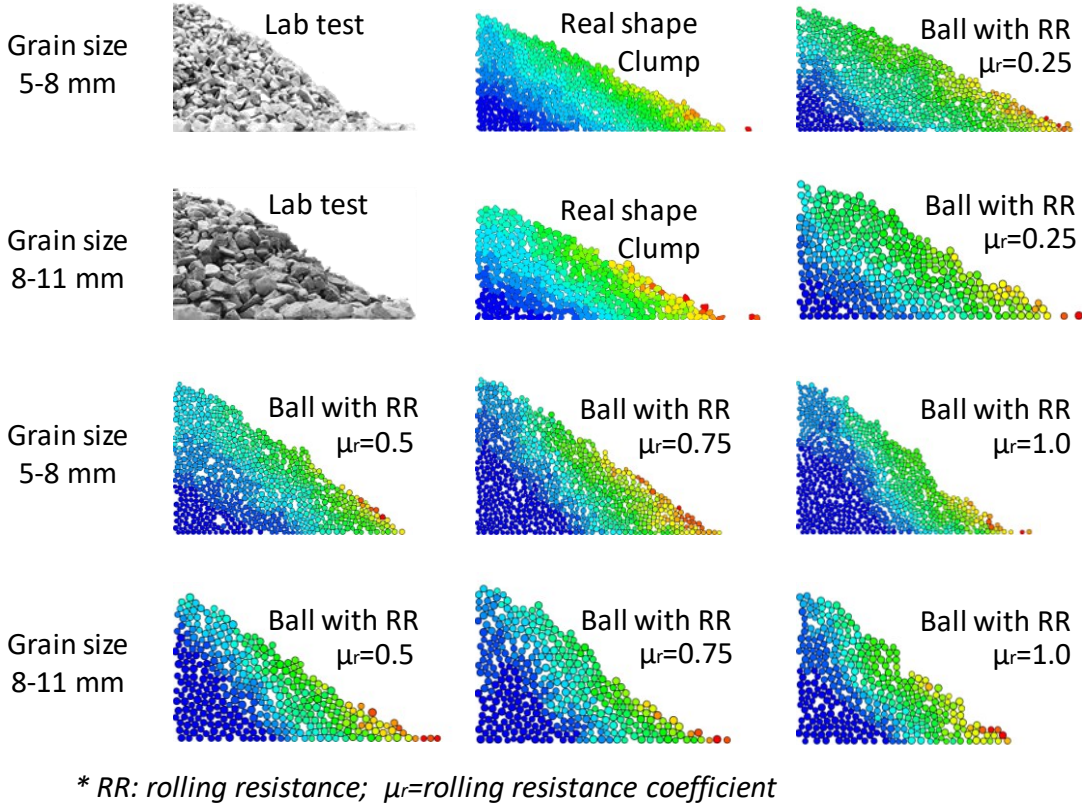
Grain size 5-8 mm — Lab test | Real shape Clump | Ball with RR $\mu_r=0.25$

Grain size 8-11 mm — Lab test | Real shape Clump | Ball with RR $\mu_r=0.25$

Grain size 5-8 mm — Ball with RR $\mu_r=0.5$ | Ball with RR $\mu_r=0.75$ | Ball with RR $\mu_r=1.0$

Grain size 8-11 mm — Ball with RR $\mu_r=0.5$ | Ball with RR $\mu_r=0.75$ | Ball with RR $\mu_r=1.0$

* RR: rolling resistance; μ_r=rolling resistance coefficient

Fig. 5 Comparison analysis of repose angle from laboratory test and simulation

At the same time, the repose angle tests in the laboratory are carried out as well. Fig. 6 compares the laboratory repose angle average value with the simulated repose angle average value with different rolling friction coefficients. Based on the measurement data in the laboratory, the variation in particle grain size has seldom affected the repose angle of particles. The data from Fig. 6 indicates the simulated results of clumps with real particle shape. The variation of its repose angle between different particle sizes matches well with the laboratory test results, and the error of the results is within 5%. However, the value of the repose angle from the clumps simulation is less than that from the lab test. The value of the gap is approximately 10°. The reason why this variation exists can be attributed to the influence of the form dimension.

On the other hand, the simulation results of spherical elements with rolling resistance perform apparent differences between 5-8 mm and 8-11 mm, varying with the results obtained from experimental measurement. Besides, the results depicted that the repose angle of larger spherical particles is significantly larger than smaller ones regardless of the rolling resistance coefficient. From this comparison analysis, it can be concluded that the simulation results of spherical elements are

inconsistent with the ones obtained from laboratory tests. In contrast, the results from clumps match the experimental one quite well.
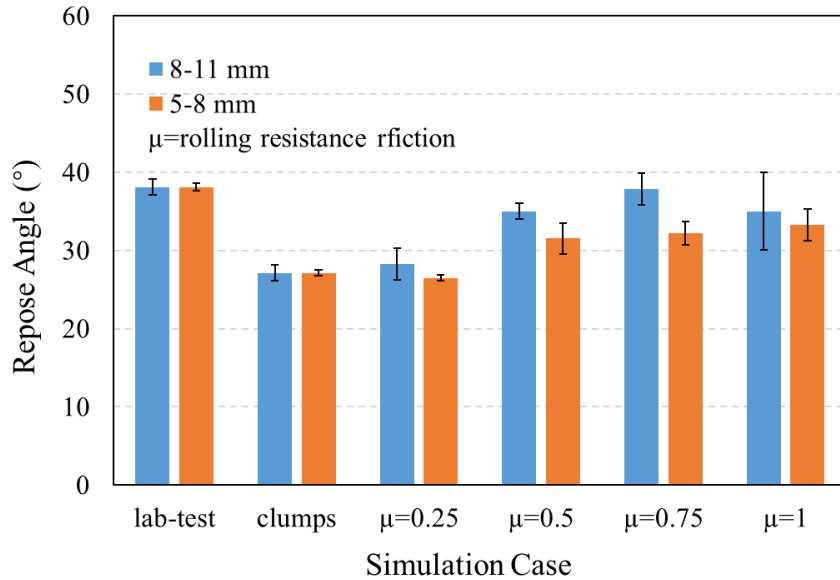

Fig. 6 Comparison analysis of the repose angle test between the laboratory and simulation results

4 Aggregate database development and extension

4.1 Development of aggregate database

The works mentioned above captured images of real coarse grains. Their parameters are extracted manually and used to reproduce the aggregate elements in DEM. This process involves a great deal of human effort (e.g., AIMS can scan 30-50 aggregates for one time, and it takes roughly one hour to collect and export the data). It has been mentioned above that the limited number of aggregates in simulation cannot represent the entire shape properties of aggregates. Therefore, it is necessary to develop the DEM aggregate database and then expand it. On the other hand, GANs method can help with reducing the processing time when enriching the DEM aggregate database. GANs can generate aggregate images according to its study and training from the existed aggregate images. These synthesized particles can be stored in the self-developed DEM Aggregate Database for further simulation. This section presents an image synthesis approach for enriching the DEM aggregate

database, using auxiliary classifier WGAN with a gradient penalty (ACWGAN-gp). A summary of this method can be seen in Fig. 7.
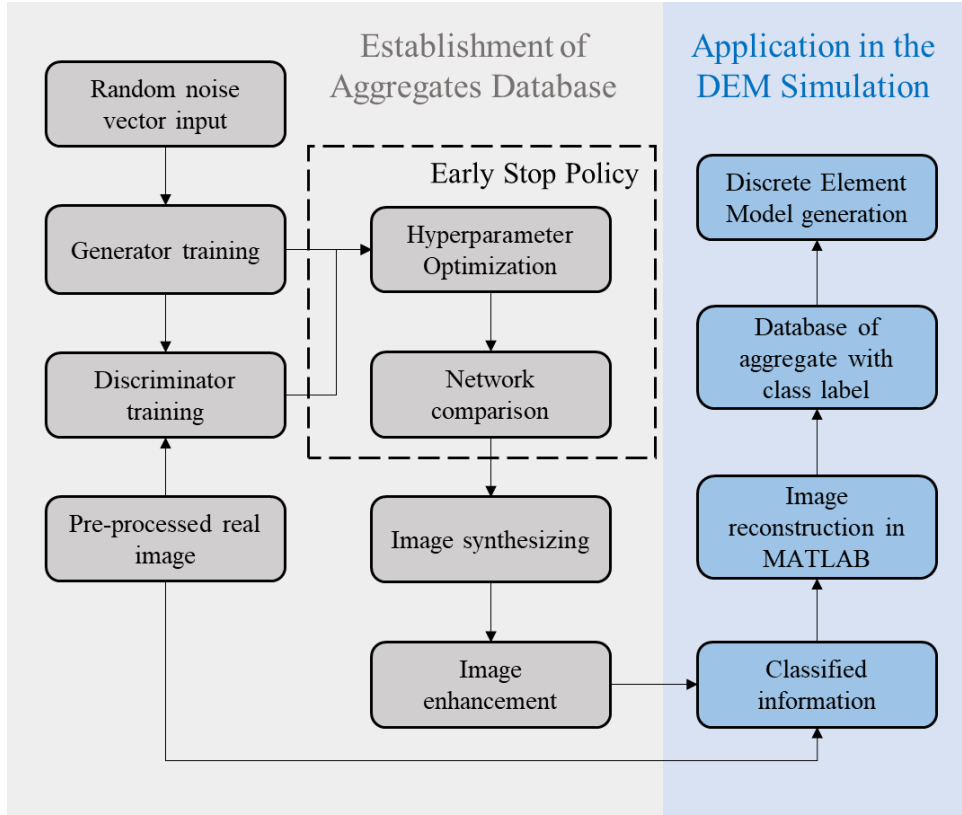

Fig. 7 Overview of Aggregate Database Development

After the model training and image synthesis, the next step is to import the aggregate image into the DEM simulation. The following sections will discuss the research strategy mentioned in Fig. *7*.

4.2 Deep learning generative models

There are two models in GANs, namely Generator Θ_G and Discriminator Θ_D. In the original GAN framework [40], the basic goal is to make Θ_D indistinguishable from the aggregated images generated by Θ_G. In the model-assisted classification GAN (ACGAN) [54], the images generated by Θ_G also have the corresponding classification labels for different aggregates including mineral type, grain size, etc. [55]. However, the original GANs model suffers from some problems that cannot be neglected. A GAN network with a cross-entropy loss function can cause the model to crash, and the computation results can be interrupted by the imbalanced capability between Θ_G and Θ_D.

Arjovsky et al. presented a new loss function on the basis of the Wasserstein distance to calculate the distance between sample distributions [42,56]. Some other scholars improved the WGAN model by gradient penalty [42]. In this way, combining the features of ACGAN and WGAN-gp, the deep learning model can synthesize images with auxiliary class information [54]. The only difference between ACGAN and ACWGAN-gp is the loss function. Fig. 8 illustrates the basic structure of how do Θ_G and Θ_D work.

Based on the estimation of Wasserstein distance between real and synthetic aggregate images, the discriminator in the network is trained to classify the image authenticity and its class labels. It can also solve the model collapse problem suffered from ordinary GANs. There will be further comparative discussion in the results section.
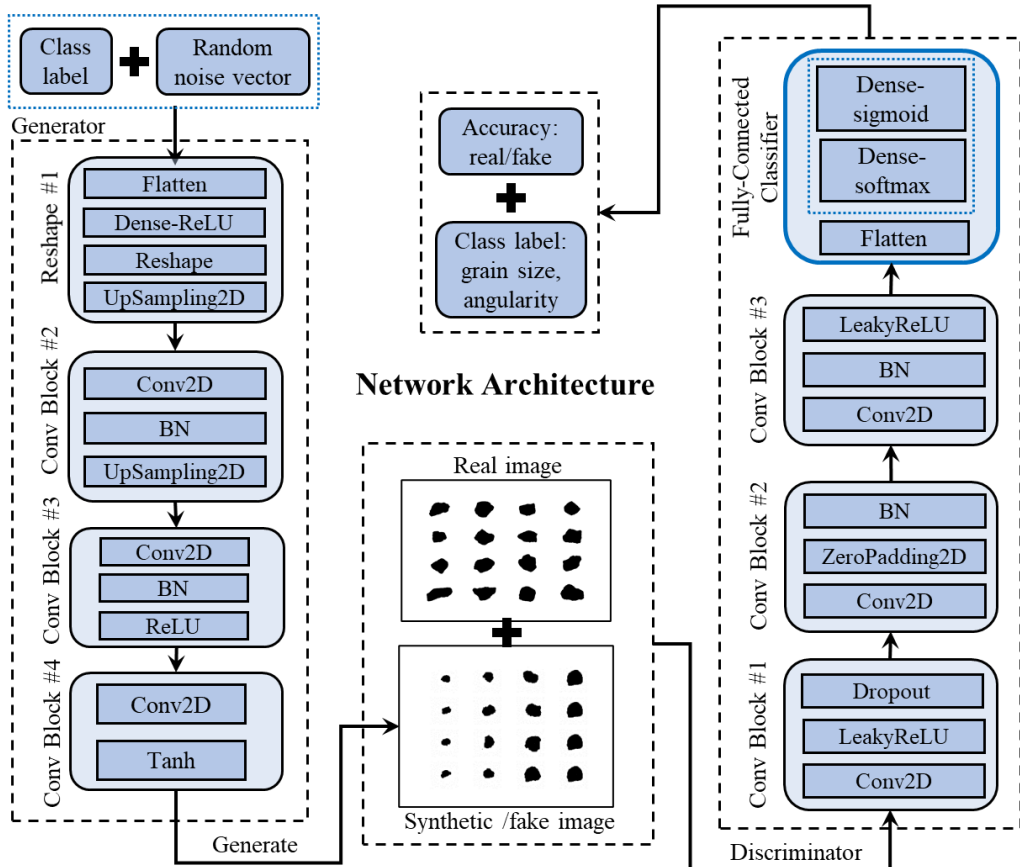

Fig. 8 Model structure of ACWGAN-gp [55]

During the training of GANs model, the loss function is mainly used to estimate the degree of variation between the real aggregate image and the synthesized (fake) one. The model's training

process keeps working until the loss function becomes convergence. On the other hand, the loss function also plays a role in calibrating the accuracy of the Generator Θ_G. The Validation of the deep learning model used in this study will be discussed in the next part.

4.3 Validation of deep learning model and database extension

Several methods are adopted to validate the model, mainly based on its built-in function (the loss function mentioned above), the model performance, and multiple-model comparison analysis.

The model performance is basically the quality and property of the aggregate images synthesized by the deep learning model. Therefore, a quantitative index of the aggregate shape is supposed to be applied to test the model performance. One of the aggregates' critical properties is the angularity that is susceptible to abrasion behavior.

The ACWGAN-gp is used to synthesize aggregate images with four different grain size categories and two different angularities "before abrasion" and "after abrasion" to test whether it can generate aggregates images with distinct angularities. The aggregate samples for the images used in this study are all from the Los Angeles Abrasion (LAA) test. This experiment can be applied to change the angularity of the aggregate [37]. The cumulative GA distribution of generated aggregate images can be seen in Fig. 9. The data analysis from this figure is mainly used to verify the accuracy of the ACWGAN-gp model on the "before wear" and "after wear" classification labels, where "BFA" represents the sample before abrasion, and "AFA" represents the data after abrasion. It can be seen from Fig. 9 that the angularity of aggregates with different grain size ranges performs a similar distribution trend. In addition, within the same range of grain size distribution, the angularities of the AFA aggregated images are dramatically smaller than those of the BFA aggregated images. It can be found from the analysis that the properties of the synthetic images are consistent with the actual test results, where all aggregates experience a sharp drop in angularity after the LAA test. Therefore, this expanded database can be used to synthesize a sufficient amount of different aggregates for the granular material simulation.
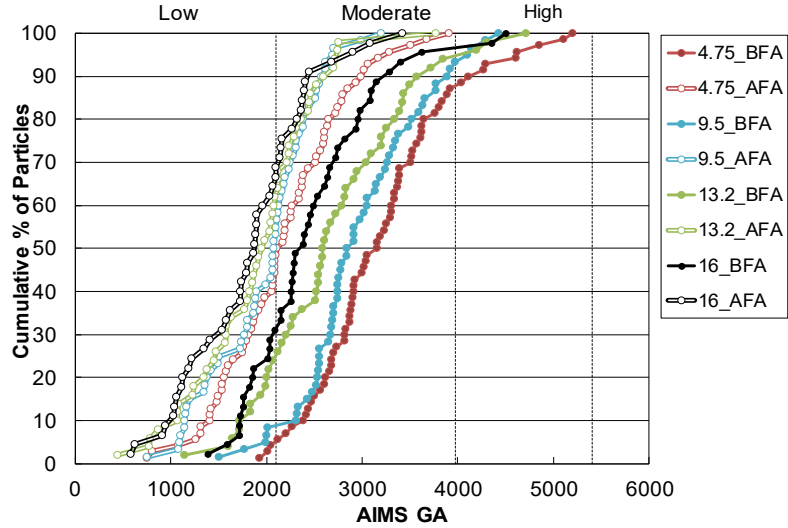
Fig. 9 Cumulative Gradient Angularity (GA) distribution of synthesized aggregates images from different grain sizes [55]

Another way to calibrate the model is multiple-model comparison analysis. t-SNE (t-Distributed Stochastic Neighbor Embedding) is used to compare the distribution of images synthesized by different GANs models, and the distribution of real images is used here as a reference. The previous study [55] presents the results for the t-SNE. And from the comparative analysis, it can be concluded that the ACWGAN-gp model is the best choice.

5 Numerical simulation of pavement pre-compation

From work mentioned above, the DEM aggregate database has been initially developed, and has been expanded through the ACWGAN-gp network. The aggregate model template is then presented in simulation and used to generate a certain number of aggregates, which can be considered as an instance. Every aggregate in the database can be imported into the simulation through the specified index as required. As shown in Fig. 10, the overall strength of the pavement layer framework is composed of interlocking between aggregates with random morphologies. Arrows of different colors and directions represent the contact force between the two polymers at the contact point, and the color of the arrow represents the value of the contact force.
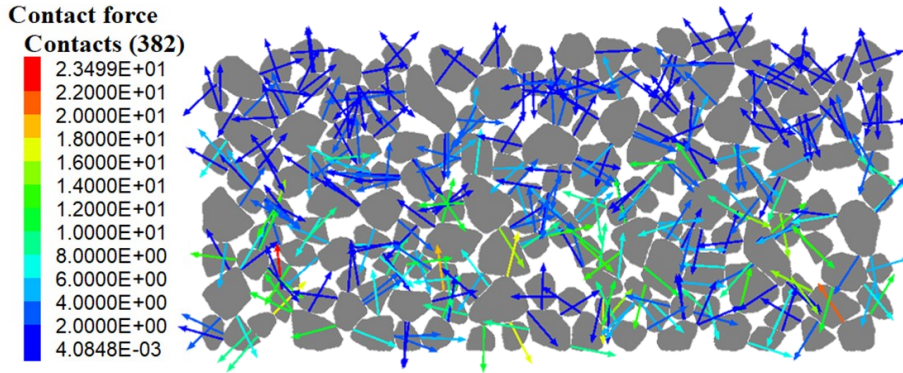
Fig. 10 Interlocking of a sub-base layer in DEM.

After the model validation and database extension, the DEM2D paving model is developed in the PFC2D based on different aggregate gradations, as shown in Fig. 11. The color of the aggregate is defined according to its displacement. It should be noted that the aggregates in this model are randomly generated from the extended database, and they have irregular distribution in the angularity. For the simplicity of the calculation, the mortar and the bitumen are removed in this model. The contact models and the parameters used in this simulation are defined according to Chapter 3. From the results in the figure, it is obvious that the movement of aggregates with a gradation of SMA-11 is more significant than that of aggregates with a gradation of AC-11. The area of aggregate rearrangement in the SMA-11 is farther forward and deeper downward. The coarse aggregates with a gradation of SMA-11 have a stronger interlocking structure during the paving compaction, transforming the external force farther and deeper into the asphalt layer. Besides, the uplift of aggregates with a gradation of SMA-11 nearby the tamper is more significant. It can be concluded from the results that compared to the graded gravel layer with a gradation of AC-11, the paver needs to move more aggregates when it compacts the layer with a gradation of SMA-11, namely it is more difficult to compact the layer with a gradation of SMA-11. For the graded gravel layer with a gradation of SMA-11, the rearrangement of coarse aggregates is better, and the compact force can be well distributed.
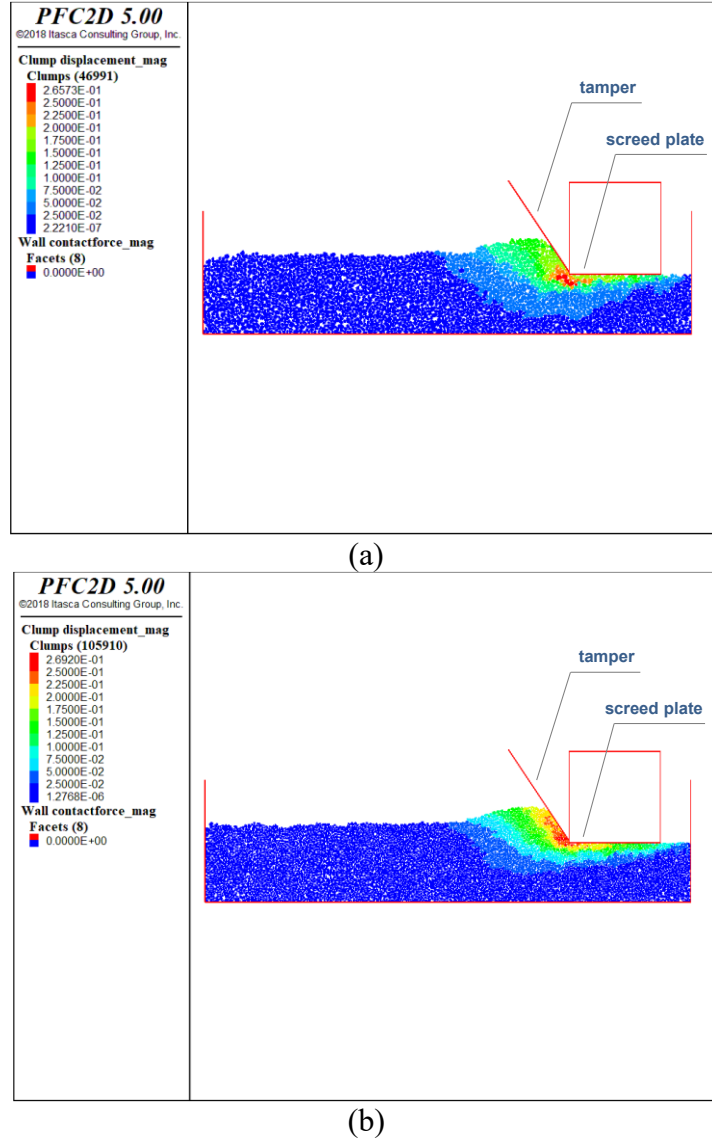
(a)

(b)

Fig. 11 Numerical simulation of DEM2D paving compaction: (a) SMA-11; (b) AC-11

The contact force between the material and tamper during paving compaction is monitored. It can be seen as Fig. 12, where the horizontal axis denotes the time step, and the vertical axis indicates the contact force. Also, the contact force between the material and screed plate during paving compaction is recorded and can be illustrated as Fig. 13. The definite integral method is used to calculate the work done by the equipment during the compaction process.
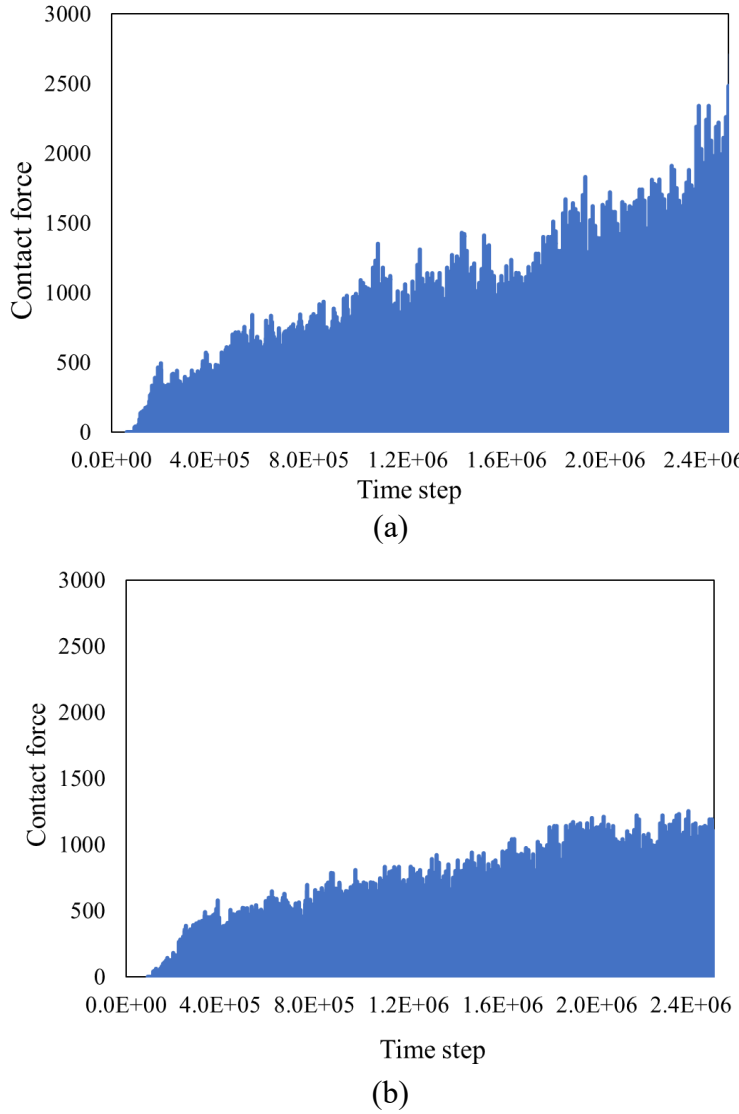
(a)

(b)

Fig. 12 Contact force between tamper and material: (a) SMA-11; (b) AC-11

From the results of the definite integral calculation in Fig. 12, the area of the figure, namely the work done by the tamper on the materials, is captured according to the figure. During the same compacting period under the same working circumstance, the work done by tamper on the SMA-11 material is 8.87E+8, and the work done by tamper on the AC-11 material is 5.42E+8. On the other hand, the work done by screed plate on the material is calculated via definite integral calculation according to Fig. *13*. During the same compacting period under the same working circumstance, the work done by tamper on the SMA-11 material is 5.85E+8, and the work done by tamper on the AC-11 material is 4.80E+8. From the results, it can be concluded that compared with AC-11, the material with a gradation of SMA-11 requires more energy to be compacted. Compared to the pavement with

19

a gradation of AC-11, the paver needs to compact and move coarser aggregates while compacting the layer with a gradation of SMA-11, so it is harder to compact the layer with a gradation of SMA-11. For the asphalt layer with a gradation of SMA-11, the rearrangement of coarse aggregates is better, and the compact force can be well distributed.

Therefore, the thermal ability of the mixture with a gradation of SMA-11 is better than the one with AC-11. Because the SMA-11 is compacted with more energy, the interlocking of coarse aggregates is more stable. In other words, the material with a gradation of SMA-11 has a better performance in high-temperature rutting resistance. The results also match the laboratory studies [5].
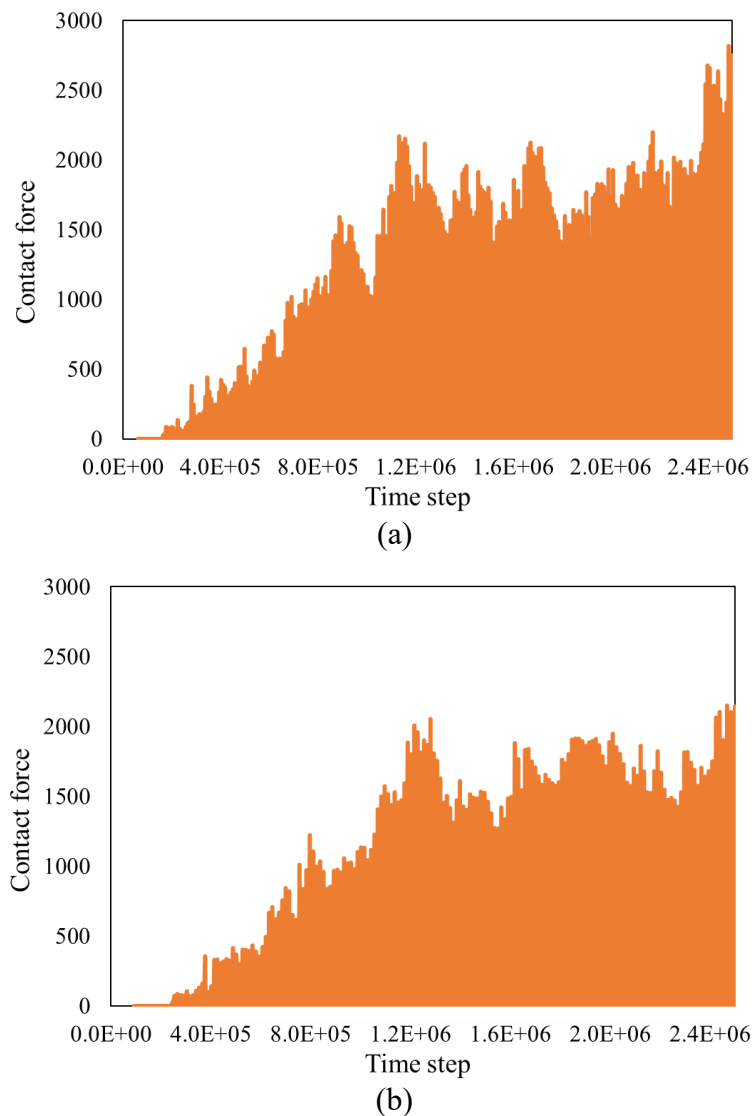

(a)

(b)

Fig. 13 Contact force between screed plate and material: (a) SMA-11; (b) AC-11

6 Conclusions and outlook

This study fulfils the development of the digital aggregate database used in DEM via the AIMS method. In addition, the GANs model is introduced to extend the existing aggregate database sourced from the fabricated process. Three different approaches are applied to calibrate the accuracy of the extended database. According to the aggregate database, the pavement paving compaction with different aggregate gradations can be simulated in DEM2D. The main conclusions and outlooks can be seen as follows:

- An innovative and integral system, being developed to simulate pavement paving compaction, is introduced in this study in detail. The aggregate database development, model expansion, and compaction simulation are described and discussed.

- These real-shape-based DEM2D aggregates are practical for studying the mechanical behavior of granular materials. And this system developed based on the DEM aggregate database can efficiently simulate the asphalt pavement paving compaction.

- The repose angle tests in the laboratory as well as in simulation are discussed in this study. From the comparison analysis, it can be concluded that the simulation results of spherical elements are inconsistent with the ones obtained from laboratory tests. In contrast, the results from clumps match the experimental one quite well.

- From the DEM2D paving simulation, it can be concluded that the thermal ability of the graded gravel layer with a gradation of SMA-11 is better than the one with AC-11. The laboratory, as well as field tests, are supposed to be conducted to verify these results.

- From the repose angle test, it can be seen that the value of repose angle from the simulation is less than that from the lab test. The value of the gap is approximately 10°. The reason why this variation exists can be attributed to the influence of the form dimension. More experiments are supposed to be conducted by authors in terms of both laboratory and field tests to further validate the calculation accuracy of the model.

7 Acknowledgments

8 Reference

[1]   S. Commuri, M. Zaman, A novel neural network-based asphalt compaction analyzer, Int. J. Pavement Eng. (2008). https://doi.org/10.1080/10298430701232018.

[2]   Y. Wan, J. Jia, Nonlinear dynamics of asphalt – screed interaction during compaction : Application to improving paving density, Constr. Build. Mater. 202 (2019) 363–373. https://doi.org/10.1016/j.conbuildmat.2018.12.205.

[3]   T.M. Ahmed, P.L. Green, H.A. Khalid, Predicting fatigue performance of hot mix asphalt using artificial neural networks, Road Mater. Pavement Des. (2017). https://doi.org/10.1080/14680629.2017.1306928.

[4]   Q. Xu, G.K. Chang, V.L. Gallivan, R.D. Horan, Influences of intelligent compaction uniformity on pavement performances of hot mix asphalt, Constr. Build. Mater. (2012). https://doi.org/10.1016/j.conbuildmat.2011.12.082.

[5]   C. Wang, M. Oeser, Z. You, Development of a material-machine cyber model for pavement paving compaction, Lehrstuhl und Institut für Straßenwesen, 2021.

[6]   Y. Ma, F. Chen, T. Ma, X. Huang, Y. Zhang, Intelligent Compaction: An Improved Quality Monitoring and Control of Asphalt Pavement Construction Technology, IEEE Trans. Intell. Transp. Syst. (2021).

[7]   Y. Ma, Y. Zhang, W. Zhao, X. Ding, Z. Wang, T. Ma, Assessment of Intelligent Compaction Quality Evaluation Index and Uniformity, J. Transp. Eng. Part B Pavements. 148 (2022) 4022024.

[8]   H. Wang, C. Wang, Z. You, X. Yang, Z. Huang, Characterising the asphalt concrete fracture performance from X-ray CT Imaging and finite element modelling, Int. J. Pavement Eng. 19 (2018) 307–318. https://doi.org/10.1080/10298436.2017.1347440.

[9]   J. Hu, P. Liu, B. Steinauer, A study on fatigue damage of asphalt mixture under different compaction using 3D-microstructural characteristics, Front. Struct. Civ. Eng. 11 (2017) 329–337. https://doi.org/10.1007/s11709-017-0407-9.

[10]   A. Abbas, E. Masad, T. Papagiannakis, T. Harman, Micromechanical Modeling of the Viscoelastic Behavior of Asphalt Mixtures Using the Discrete-Element Method, Int. J. Geomech. (2007). https://doi.org/10.1061/(asce)1532-3641(2007)7:2(131).

[11]   Y. Liu, Z. You, Discrete-Element Modeling: Impacts of Aggregate Sphericity, Orientation, and Angularity on Creep Stiffness of Idealized Asphalt Mixtures, J. Eng. Mech. (2011). https://doi.org/10.1061/(asce)em.1943-7889.0000228.

[12]   H. Ding, H. Wang, X. Qu, A. Varveri, J. Gao, Z. You, Towards an understanding of diffusion mechanism of bio-rejuvenators in aged asphalt binder through molecular dynamics simulation, J. Clean. Prod. 299 (2021) 126927.

[13]   S. Huschek, Zum Verformungsverhalten von Asphaltbeton unter Druck, (1983).

[14]   P. Liu, H. Xu, D. Wang, C. Wang, C. Schulze, M. Oeser, Comparison of mechanical responses of asphalt mixtures manufactured by different compaction methods, Constr. Build. Mater. (2018). https://doi.org/10.1016/j.conbuildmat.2017.12.082.

[15]   F. Otto, Dynamisches Interaktionsverhalten zwischen Oszillationsbandagen und Asphaltoberflächen, RWTH Aachen University, 2020.

[16] X. Zhou, S. Chen, D. Ge, D. Jin, Z. You, Investigation of asphalt mixture internal structure consistency in accelerated discrete element models, Constr. Build. Mater. (2020). https://doi.org/10.1016/j.conbuildmat.2020.118272.

[17] P.A. Cundall, O.D.L. Strack, Discrete Numerical Model for Granualr Assemblies, Geotechnique. (1979).

[18] P.A. Cundall, O.D.L. Strack, Modeling of microscopic mechanisms in granular material, in: Stud. Appl. Mech., 1983. https://doi.org/10.1016/B978-0-444-42192-0.50018-9.

[19] Y. Liu, X. Zhou, Z. You, B. Ma, F. Gong, Determining Aggregate Grain Size Using Discrete-Element Models of Sieve Analysis, Int. J. Geomech. 19 (2019) 04019014. https://doi.org/10.1061/(asce)gm.1943-5622.0001376.

[20] J.P. Bardet, Q. Huang, Numerical modeling of micropolar effects in idealized granular materials, Mech. Granul. Mater. Powder Syst. 37 (1992) 85–92.

[21] E. Olsson, D. Jelagin, M.N. Partl, New discrete element framework for modelling asphalt compaction, Road Mater. Pavement Des. (2019) 1–13. https://doi.org/10.1080/14680629.2019.1633750.

[22] Y. Gao, Y. Zhang, F. Gu, T. Xu, H. Wang, Impact of minerals and water on bitumen-mineral adhesion and debonding behaviours using molecular dynamics simulations, Constr. Build. Mater. 171 (2018) 214–222.

[23] Y. Gao, L. Li, Y. Zhang, Modelling crack initiation in bituminous binders under a rotational shear fatigue load, Int. J. Fatigue. 139 (2020) 105738.

[24] Y. Gao, L. Li, Y. Zhang, Modeling crack propagation in bituminous binders under a rotational shear fatigue load using pseudo J-integral Paris' law, Transp. Res. Rec. 2674 (2020) 94–103.

[25] J. Hu, T. Ma, Y. Zhu, X. Huang, J. Xu, A feasibility study exploring limestone in porous asphalt concrete: Performance evaluation and superpave compaction characteristics, Constr. Build. Mater. 279 (2021) 122457.

[26] F. Tang, T. Ma, J. Zhang, Y. Guan, L. Chen, Integrating three-dimensional road design and pavement structure analysis based on BIM, Autom. Constr. 113 (2020) 103152.

[27] D. Ge, D. Jin, C. Liu, J. Gao, M. Yu, L. Malburg, Z. You, Laboratory Performance and Field Case Study of Asphalt Mixture with Sasobit Treated Aramid Fiber as Modifier, Transp. Res. Rec. (2021) 03611981211047833.

[28] F. Ash, X. Zhao, D. Ge, J. Wang, D. Wu, J. Liu, Mixture Containing Municipal Solid Waste Incineration, (2022).

[29] Y. Gao, M. Dong, L. Li, L. Wang, Z. Sun, Interface effects on the creep characteristics of asphalt concrete, Constr. Build. Mater. 96 (2015) 591–598.

[30] Y. Gao, Y. Zhang, Y. Yang, J. Zhang, F. Gu, Molecular dynamics investigation of interfacial adhesion between oxidised bitumen and mineral surfaces, Appl. Surf. Sci. 479 (2019) 449–462.

[31] Y. Zhang, Y. Gao, Predicting crack growth in viscoelastic bitumen under a rotational shear fatigue load, Road Mater. Pavement Des. 22 (2021) 603–622.

[32] E. Olsson, D. Jelagin, M.N. Partl, New discrete element framework for modelling asphalt compaction, Road Mater. Pavement Des. 20 (2019) 604–616. https://doi.org/10.1080/14680629.2019.1633750.

[33] L. Li, M. Begbie, G. Brown, D. Uttamchandani, Design, simulation and characterization of a MEMS optical scanner, J. Micromechanics Microengineering. 17 (2007) 1781.

[34] C.H. Trinderup, V.A. Dahl, K.M. Gregersen, L.A.A. Orlando, A.B. Dahl, The Traveling Optical Scanner–Case Study on 3D Shape Models of Ancient Brazilian Skulls, in: Int. Conf. Image Signal Process., Springer, 2016: pp. 398–405.

[35] Y. Liu, F. Gong, Z. You, H. Wang, Aggregate morphological characterization with 3D optical scanner versus X-ray computed tomography, J. Mater. Civ. Eng. (2018). https://doi.org/10.1061/(ASCE)MT.1943-5533.0002091.

[36] E.A. Masad, Aggregate Imaging System (AIMS): Basics and Applications, Austin, Texas 78763-5080, 2005.

[37] C. Wang, H. Wang, M. Oeser, M.R. Mohd Hasan, Investigation on the morphological and mineralogical properties of coarse aggregates under VSI crushing operation, Int. J. Pavement Eng. (2020) 1–14. https://doi.org/10.1080/10298436.2020.1714043.

[38] W. Deng, Y. Mou, T. Kashiwa, S. Escalera, K. Nagai, K. Nakayama, Y. Matsuo, H. Prendinger, Vision based pixel-level bridge structural damage detection using a link ASPP network, Autom. Constr. (2020). https://doi.org/10.1016/j.autcon.2019.102973.

[39] K. Zhang, Y. Zhang, H.-D. Cheng, CrackGAN: A Labor-Light Crack Detection Approach Using Industrial Pavement Images Based on Generative Adversarial Learning, XX (2019) 1–13. http://arxiv.org/abs/1909.08216.

[40] I.J. Goodfellow, J. Pouget-Abadie, M. Mirza, B. Xu, D. Warde-Farley, S. Ozair, A. Courville, Y. Bengio, Generative adversarial nets, in: Adv. Neural Inf. Process. Syst., 2014. https://doi.org/10.3156/jsoft.29.5_177_2.

[41] T. Salimans, I. Goodfellow, W. Zaremba, V. Cheung, A. Radford, X. Chen, Improved techniques for training GANs, in: Adv. Neural Inf. Process. Syst., 2016.

[42] I. Gulrajani, F. Ahmed, M. Arjovsky, V. Dumoulin, A. Courville, Improved training of wasserstein GANs, in: Adv. Neural Inf. Process. Syst., 2017.

[43] Z. Fan, Y. Wu, J. Lu, W. Li, Automatic Pavement Crack Detection Based on Structured Prediction with the Convolutional Neural Network, (2018) 1–9. http://arxiv.org/abs/1802.02208.

[44] K. Gopalakrishnan, Deep learning in data-driven pavement image analysis and automated distress detection: A review, Data. (2018). https://doi.org/10.3390/data3030028.

[45] R. Li, Z. Leng, Y. Zhang, X. Ma, Preparation and characterization of waterborne epoxy modified bitumen emulsion as a potential high-performance cold binder, J. Clean. Prod. 235 (2019) 1265–1275. https://doi.org/10.1016/j.jclepro.2019.06.267.

[46]   C. Wang, M. Moharekpour, Q. Liu, Z. Zhang, P. Liu, M. Oeser, Investigation on asphalt-screed interaction during pre-compaction: Improving paving effect via numerical simulation, Constr. Build. Mater. 289 (2021) 123164.

[47]   X. Yang, Q. Dai, Z. You, Z. Wang, Integrated Experimental-Numerical Approach for Estimating Asphalt Mixture Induction Healing Level through Discrete Element Modeling of a Single-Edge Notched Beam Test, J. Mater. Civ. Eng. (2015). https://doi.org/10.1061/(asce)mt.1943-5533.0001231.

[48]   S. Chen, Z. You, S.-L. Yang, A. Garcia, L. Rose, Influence of air void structures on the coefficient of permeability of asphalt mixtures, Powder Technol. 377 (2021) 1–9.

[49]   C. Wang, P. Liu, M. Oeser, X. Zhou, H. Wang, Simulation of granular material in Distinct Element Model based on real particle shape, in: Adv. Mater. Pavement Perform. Predict. II Contrib. to 2nd Int. Conf. Adv. Mater. Pavement Perform. Predict. (AM3P 2020), 27-29 May, 2020, San Antonio, TX, USA, CRC Press, 2020: p. 109.

[50]   E.M. Ortiz, E. Mahmoud, Experimental procedure for evaluation of coarse aggregate polishing resistance, Transp. Geotech. (2014). https://doi.org/10.1016/j.trgeo.2014.06.001.

[51]   E. Masad, T. Fletcher., Aggregate imaging system (AIMS): basics and application, 2005.

[52]   H. Wang, D. Wang, P. Liu, J. Hu, C. Schulze, M. Oeser, Development of morphological properties of road surfacing aggregates during the polishing process, Int. J. Pavement Eng. (2017). https://doi.org/10.1080/10298436.2015.1088153.

[53]   I. Cavers, An Introductory Guide to MATLAB, Dep. Comput. Sci. Univ. Br. Columbia. 4 (1998).

[54]   A. Iyer, B. Dey, A. Dasgupta, W. Chen, A. Chakraborty, A Conditional Generative Model for Predicting Material Microstructures from Processing Methods, (2019). http://arxiv.org/abs/1910.02133.

[55] C. Wang, F. Li, Q. Liu, H. Wang, P. Benmoussa, S. Jeschke, M. Oeser, Establishment and extension of digital aggregate database using auxiliary classifier Wasserstein GAN with gradient penalty, Constr. Build. Mater. 300 (2021) 124217.

[56] I. Gulrajani, F. Ahmed, M. Arjovsky, V. Dumoulin, A. Courville, Improved Wasserstein GANs, Aquat. Procedia. (2017). https://doi.org/10.1016/j.aqpro.2013.07.003.